INTERNSHIP REPORT

June 9th 2025 – September 26th 2025

A Study of Thermo-Chemical Non-Equilibrium and Radiation in Hypersonic Re-entry Vehicles Using Computational Fluid Dynamics

APPLIED TO THE STARDUST TEST CASE

September 25, 2025

Author:

Justine Brun

Supervised by:

Jan Vos

Contents

Abstract **1**

List of Figures **1**

List of Tables **1**

1 Introduction **2**

2 Stardust reentry capsule **3**

3 Simulation configuration **4**
- 3.1 Geometry & meshing 4
- 3.2 The NSMB solver 4
- 3.3 Numerical parameters 5
- 3.4 Flow model 5
- 3.5 Kinetic model 5
  - 3.5.1 Chemical species 6
  - 3.5.2 Chemical reactions 6
  - 3.5.3 Mass fractions 7
- 3.6 Thermo-chemical models 7
- 3.7 Boundary conditions 7

4 Numerical simulation results **7**
- 4.1 Conditions for Stardust test cases 8
- 4.2 Flow property contours along the capsule skin 8
- 4.3 Surface viscosity 9
- 4.4 Surface forebody pressure distributions 9
- 4.5 Temperature distributions along the stagnation streamline 10
- 4.6 Heat flux distribution along the capsule skin 11
- 4.7 Mass fraction distributions along the stagnation streamline 12
- 4.8 3D geometry 13
- 4.9 TPS ablation 15

5 Conclusions **15**

Abstract

This report presents a numerical study of thermo-chemical non-equilibrium and radiative effects in hypersonic re-entry flows, with a focus on the Stardust flight experiment conducted by NASA. Employing the NSMB (Navier–Stokes Multi-Block) solver and an 11-species air model, simulations were conducted under conditions representative of the Stardust mission's peak heating phase.

Results from the numerical simulations are compared with well-developed codes to evaluate the predictive capability of the different modeling approaches. articular emphasis is placed on the role of chemical and thermal non-equilibrium, grid resolution, and surface conditions, including wall catalyticity and radiative heat transfer.

Comparisons with prior numerical studies demonstrate good agreement, especially near the stagnation region. The findings underscore the importance of incorporating thermo-chemical non-equilibrium and radiation modeling for accurate heat flux predictions and highlight the challenges of validating flowfield quantities in the absence of direct measurements.

List of Figures

1 Stardust capsule after landing in Utah on January 15, 2006 2
2 Stardust capsule configuration 3
3 Modeling of the Stardust geometry 4
4 Overview of the baseline grid used 4
5 Flowfield results obtained with the 11-species air model using Park's 1989 non-equilibrium chemistry model 8
6 Surface viscosity 9
7 Surface forebody pressure profiles for various wall conditions 10
8 Temperature profiles along the stagnation line 10
9 Total wall heat flux for various wall conditions 11
10 Mass fraction profiles along the stagnation streamline 12
11 3D mesh 13
12 Wall heat flux profiles for different viscosity models 14
13 Wall heat flux profiles for different surface chemistry models 14

List of Tables

1 Numerical parameters used for laminar and inviscid simulations 5
2 Chemical species considered in the 11-species air model 6
3 Initial mass fractions at the inflow boundary 7
4 Conditions for Stardust test case 8

1 Introduction

The accurate prediction of hypersonic flow phenomena during atmospheric re-entry is crucial for the design and safe operation of spacecraft. One key challenge is modeling the complex thermo-chemical processes that govern the behavior of the shock layer formed around the vehicle.

Hypersonic flows at Mach numbers on the order of 20, typical of re-entry trajectories, result in extreme aerodynamic heating and strong shock waves. These conditions cause the atmospheric gas to dissociate and partially ionize in the shock-compressed layer near the vehicle surface. In addition to convective heating, significant radiative heat transfer can also occur, especially at high altitudes where the gas becomes optically thin. The intensity of these physico-chemical processes varies significantly with altitude.

Figure 1: Stardust capsule after landing in Utah on January 15, 2006

This report focuses on the atmospheric reentry of the Stardust sample return capsule, a mission conducted by the National Aeronautics and Space Administration (NASA) to collect and return cometary and interstellar dust to Earth. The Stardust capsule's reentry on January 15, 2006, represents one of the fastest Earth reentries of a spacecraft to date, occurring at approximately 12.9 km/s. This extreme velocity led to a severe aerothermal environment, making it a valuable case for studying non-equilibrium hypersonic flow phenomena. The comprehensive dataset associated with the mission, including surface heat-flux measurements and radiative heating estimates, serves as an important benchmark for validating computational tools that model high-enthalpy, chemically reacting flows.

The numerical methodology employed here involves solving the Navier–Stokes equations coupled with detailed thermo-chemical non-equilibrium models for laminar flow cases, and the Euler equations for inviscid flow cases. Both flow regimes are investigated using two mesh resolutions: a baseline grid and a refined grid. This allows for a comparative assessment of the effect of mesh resolution on the predicted results, enabling a loose evaluation of grid convergence behavior.

The objectives of this work include validating simulation results against available flight data, with a particular focus on surface heat-transfer rates and radiation. Additionally, the study examines predicted mass fractions and temperatures along the stagnation streamline to assess the sensitivity of the results to both the physical modeling approach (laminar vs. inviscid) and mesh refinement, despite the limited availability of experimental data for internal flowfield quantities.

2 Stardust reentry capsule

The Stardust sample return capsule was part of a NASA mission to collect and return cometary and interstellar dust, becoming the first U.S. spacecraft to return material from beyond the Moon. The capsule reentered Earth's atmosphere on January 15, 2006, at a velocity of approximately 12.9 km/s—making it one of the fastest Earth reentries to date. This extreme velocity produced a highly energetic, chemically reacting flowfield, offering a unique opportunity to study real-gas effects, strong shock-layer radiation, and ablation phenomena under high-enthalpy conditions.

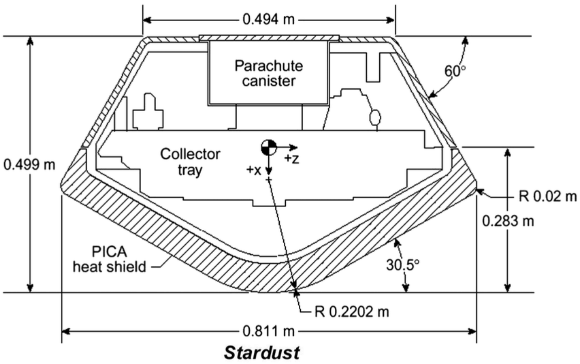

Figure 2: Stardust capsule configuration

The spacecraft's Thermal Protection System (TPS) consisted of a PICA (Phenolic Impregnated Carbon Ablator) heat shield, which underwent significant ablation during reentry. Although no onboard sensors measured heat flux directly, post-flight analysis and ground-based testing—including arc-jet experiments—enabled estimation of surface recession, heat flux, and radiative contributions. These reconstructions, combined with trajectory data, provide valuable benchmarks for validating high-fidelity CFD models of non-equilibrium, ablating flows.

The Stardust case has been examined in the literature by various researchers. Notably, Mitcheltree et al. [7] performed early aerodynamic analyses to support capsule design and trajectory planning. Desai et al. [3] focused on the entry, descent, and landing (EDL) operations, providing critical trajectory and mission context. Gupta [4] and Olynick et al. [5] conducted coupled radiation and ablation simulations, contributing to the understanding of thermal protection system (TPS) response under high-enthalpy conditions. More recently, Trumble et al. [6] presented a postflight aerothermal analysis based on trajectory data and material response models. These works serve as valuable references for validating current CFD tools and physical models used in simulating Stardust reentry conditions.

This work aims to simulate a selected point along the Stardust reentry trajectory using the CFD code NSMB, with particular emphasis on surface heat-transfer rates and the role of modeling assumptions such as viscous effects, chemical nonequilibrium, and grid resolution. Results are compared against those available in the literature to assess model accuracy and mesh sensitivity.

3 Simulation configuration

3.1 Geometry & meshing

The Stardust vehicle was modeled using an axi-symmetric approximation, consistent with its geometry and the absence of angle of attack during the flight. This simplification reduces computational cost while preserving the essential physical features of the flow. A structured mesh was used to discretize the flow domain. The mesh was designed to resolve the bow shock and the boundary layer with sufficient accuracy.

Two mesh resolutions were considered for the simulations: a baseline grid and a refined grid. The refined grid includes a higher density of points near the stagnation region and along the body surface to better capture various gradients.

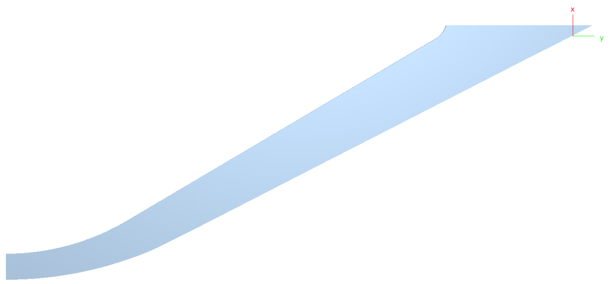

Figure 3: Modeling of the Stardust geometry

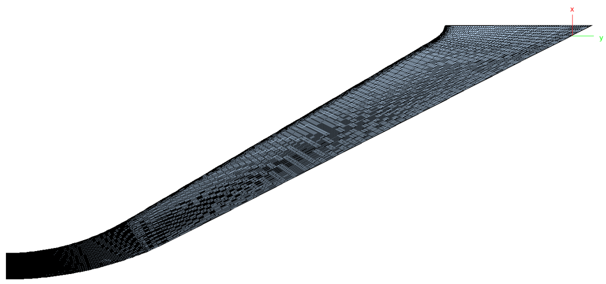

Figure 4: Overview of the baseline grid used

Figure 3 shows the 2D modeling of the Stardust geometry, while Figure 4 provides an overview of the baseline computational mesh used in the simulations.

3.2 The NSMB solver

All CFD computations in this study were performed using the Navier–Stokes Multi Block (NSMB) solver, developed by a consortium of universities and industry partners [1]. NSMB is a parallelized, cell-centered finite volume solver designed for compressible flows on structured multi-block grids.

The code supports both explicit and implicit time integration schemes, with second- and fourth-order central discretizations (with artificial dissipation), as well as several upwind schemes up to fifth order. Turbulence modeling includes validated RANS models (up to 5 equations), LES, hybrid RANS–LES, and transition models.

NSMB was originally developed with hypersonic applications in mind, such as atmospheric re-entry. It includes various levels of chemical modeling for air, CO_2, and N_2, with available air models incorporating 5, 7, 11, or 13 species. Non-equilibrium models include those by Park (1989–2001), Gardiner, and Dunn–Kang, using equilibrium constants computed from polynomial fits (further details available in [1]).

Thermo-chemical non-equilibrium is modeled via the Landau–Teller theory for translational – vibrational energy exchange, with Millikan–White relaxation times. Transport coefficients are computed using the Blottner model or the Gupta-Yos model. Both inviscid and viscous flows (laminar and turbulent) are supported. Wall boundary conditions allow for super- and partially catalytic surfaces.

NSMB has been employed extensively in various European projects, demonstrating its versatility and robustness across a range of aerodynamic applications.

3.3 Numerical parameters

The numerical parameters employed for the laminar and inviscid simulations (for both baseline and refined grids) are summarized in Table 1.

Model	Number of time steps (`NSTEPS`)	CFL number
Laminar	40 000	0.25
Inviscid	35 000	0.1

Table 1: Numerical parameters used for laminar and inviscid simulations

For spatial discretization, a second-order upwind AUSMDV (Advection Upstream Splitting Method - Ducros and Vielle) and Haenel hybrid scheme was used for all models. This approach combines flux-vector splitting with additional dissipation control to enhance stability and accuracy in regions with strong gradients.

3.4 Flow model

The atmosphere is considered as a continuum since the Knudsen number is less than 0.01. Specifically :

$$\mathrm{Kn} = \frac{\lambda}{L} \approx 0.00255 \quad \text{with} \quad \begin{cases} \lambda = 0.583 \cdot 10^{-3}\,\mathrm{m}\text{: mean free path} \\ L = R_n = 22.86\,\mathrm{cm}\text{: capsule's characteristic length} \end{cases}$$

The simulations were conducted under the assumption of steady-state conditions. A laminar flow model was employed, appropriate for the flow regime under consideration. Viscous effects were modeled using the Blottner viscosity model with the Eucken correction to account for the thermal conductivity effects.

3.5 Kinetic model

The assumption of a quiescent, chemically frozen atmosphere at inflow is applied. The following assumptions are made at the inflow boundary:

- The air is considered a reacting gas mixture, composed of multiple species, including both neutral and ionized components.

- The inflow temperature and pressure are such that only the major neutral species (N_2, O_2) are present in significant amounts, while minor species and ionized components are initialized at trace concentrations.
- A fixed 11-species air model is used for all simulations. The number of species is not the main focus of the present study but was selected to capture the relevant thermochemical nonequilibrium effects.

3.5.1 Chemical species

The chemical species considered are summarized in Table 2.

11-species air model
Molecular nitrogen (N_2)
Molecular oxygen (O_2)
Nitric oxide (NO)
Atomic nitrogen (N)
Atomic oxygen (O)
Ionized nitric oxide (NO^+)
Ionized molecular nitrogen (N_2^+)
Ionized molecular oxygen (O_2^+)
Atomic nitrogen ion (N^+)
Atomic oxygen ion (O^+)
Electron (e^-)

Table 2: Chemical species considered in the 11-species air model

3.5.2 Chemical reactions

In this work, we will primarily focus on the 11-species air model. Accordingly, the following reactions, including dissociation, recombination, ionization and charge exchange processes, are considered (as reported in [2]):

$$\mathrm{N_2 + M \rightleftharpoons 2N + M} \tag{1}$$
$$\mathrm{O_2 + M \rightleftharpoons 2O + M} \tag{2}$$
$$\mathrm{NO + M \rightleftharpoons N + O + M} \tag{3}$$
$$\mathrm{N_2 + O \rightleftharpoons NO + N} \tag{4}$$
$$\mathrm{NO + O \rightleftharpoons O_2 + N} \tag{5}$$
$$\mathrm{N + O \rightleftharpoons NO^+ + } e^- \tag{6}$$
$$\mathrm{N + N \rightleftharpoons N_2^+ + } e^- \tag{7}$$
$$\mathrm{O + O \rightleftharpoons O_2^+ + } e^- \tag{8}$$
$$\mathrm{N} + e^- \rightleftharpoons \mathrm{N^+} + 2e^- \tag{9}$$
$$\mathrm{O} + e^- \rightleftharpoons \mathrm{O^+} + 2e^- \tag{10}$$
$$\mathrm{N_2 + O_2^+ \rightleftharpoons N_2^+ + O_2} \tag{11}$$
$$\mathrm{NO^+ + N \rightleftharpoons O^+ + N_2} \tag{12}$$
$$\mathrm{NO^+ + O \rightleftharpoons N^+ + O_2} \tag{13}$$
$$\mathrm{NO^+ + O_2 \rightleftharpoons NO + O_2^+} \tag{14}$$
$$\mathrm{NO^+ + N \rightleftharpoons N_2^+ + O} \tag{15}$$
$$\mathrm{O_2^+ + N \rightleftharpoons N^+ + O_2} \tag{16}$$
$$\mathrm{O^+ + NO \rightleftharpoons NO^+ + O} \tag{17}$$
$$\mathrm{NO^+ + O \rightleftharpoons O_2^+ + N} \tag{18}$$
$$\mathrm{O^+ + N_2 \rightleftharpoons N_2^+ + O} \tag{19}$$

where M represents any species acting as a third body to conserve energy and momentum.

3.5.3 Mass fractions

We assume the atmosphere's air has the composition presented in Table 3.

Species	Mass fraction
N_2	0.76536
O_2	0.23464
N	1×10^{-12}
NO	1×10^{-12}
O	1×10^{-12}
NO^+	1×10^{-12}
N_2^+	1×10^{-12}
O_2^+	1×10^{-12}
N^+	1×10^{-12}
O^+	1×10^{-12}
e^-	1×10^{-12}

Table 3: Initial mass fractions at the inflow boundary

3.6 Thermo-chemical models

The kinetic model employed in this study accounts for thermo-chemical non-equilibrium effects, typical of hypersonic flow environments. These effects arise at high speeds and altitudes when the characteristic flow time around a hypersonic vehicle is comparable to or shorter than the time required for molecular collisions to restore equilibrium.

To model the vibrational relaxation behavior of diatomic molecules, Millikan-White's empirical model was considered for the vibrational relaxation time. Chemical non-equilibrium effects are captured using `gas model 4`, while thermo-chemical non-equilibrium, where both chemical kinetics and internal energy mode relaxation are treated in a coupled manner, is modeled using `gas model 5`.

3.7 Boundary conditions

The inflow boundary conditions correspond to the free-stream conditions reported in [4], [7], and [5] for the Stardust reentry at peak heating. The wall temperature is fixed at $T_{\text{wall, inv}} = 1\,000\,\text{K}$ and $T_{\text{wall, lam}} = 3\,800\,\text{K}$ for the inviscid and laminar configurations, respectively. Additionally, thermal equilibrium between the vibrational and wall temperatures is assumed at the streamlined surface, i.e., $T_{\text{vib}} = T_{\text{wall}}$.

Ablation is not considered in the present study.

4 Numerical simulation results

The flow field is simulated using NSMB with different thermo-chemical models and the results are compared to previous investigations in terms of temperature, pressure, species number density, wall heat flux and radiation. It should also be noted that the reference curves from the literature were not available in electronic format and were therefore digitized manually. As a result, some uncertainty and limited precision should be considered when interpreting these comparisons.

4.1 Conditions for Stardust test cases

Table 4 presents the initial data for the numerical modeling at $t = 54\,\text{s}$ as described in [4] and [5]. All input files were initialized using these conditions.

Altitude (km)	u_∞ (km/s)	T_∞ (K)	ρ_∞ (kg/m^3)
59.77	11.14	238.47	$2.34 \cdot 10^{-4}$

Table 4: Conditions for Stardust test case

The air model is fixed to 11 species in both chemical and thermo-chemical non-equilibrium based on Park's 1989 chemistry model, consistent with the references used for comparison.

4.2 Flow property contours along the capsule skin

The contours in Figure 5 illustrate key flow properties along the capsule skin and, in particular, capture the expansion phenomenon occurring downstream of the capsule's shoulder as seen in Figure 5c.

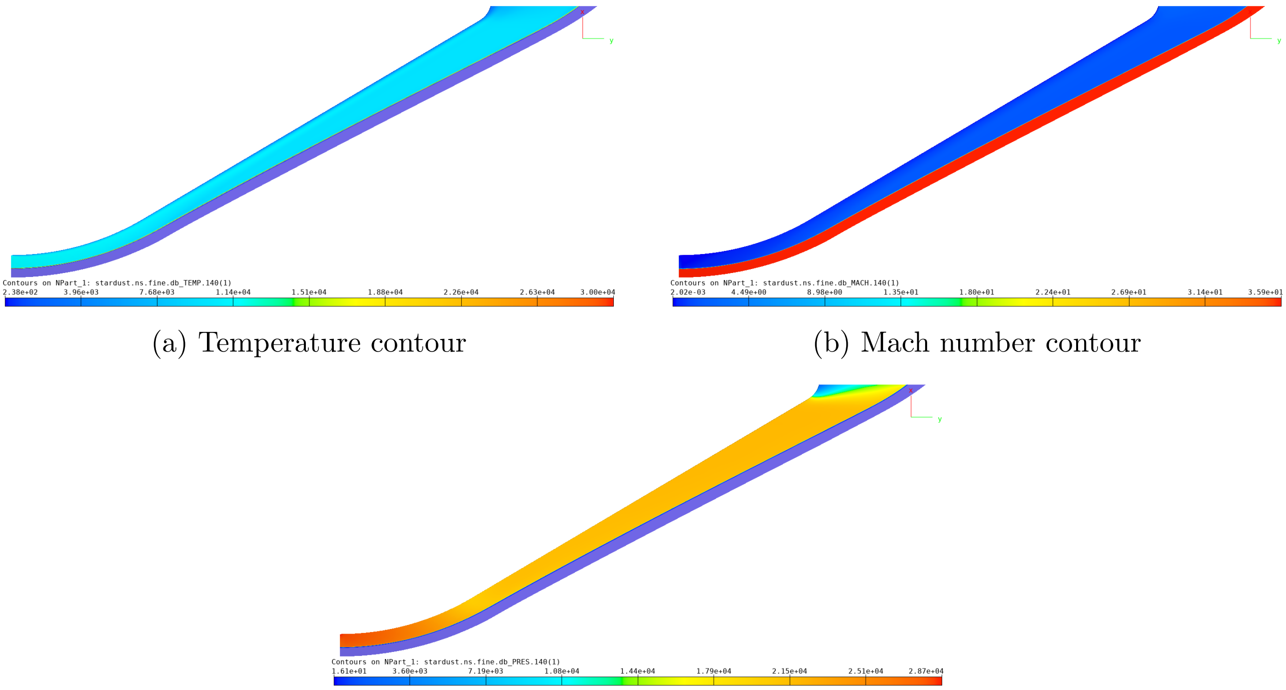

(a) Temperature contour

(b) Mach number contour

(c) Pressure contour

Figure 5: Flowfield results obtained with the 11-species air model using Park's 1989 non-equilibrium chemistry model

Similar contours are observed for the other models, with only minor variations in the values and slight differences in the shock layer thickness.

4.3 Surface viscosity

The distribution of dynamic viscosity along the capsule surface is shown in Figure 6. As expected, viscosity increases toward the stagnation region due to the elevated temperatures, then decreases along the shoulder as the flow expands and cools. These trends are consistent with the expected behavior in chemically reacting, non-equilibrium hypersonic boundary layers.

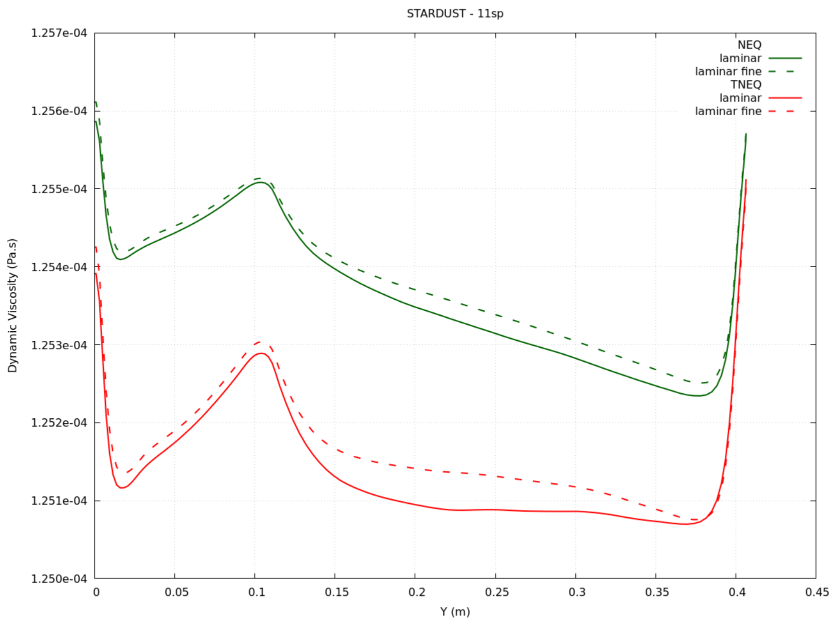

Figure 6: Surface viscosity

The maximum dynamic viscosity of approximately 1.309×10^{-4} Pa · s indicates that viscous effects, especially near the stagnation region, are significant. Because heat transfer to the wall is strongly influenced by the boundary layer behavior, inviscid simulations alone cannot capture the thermal loads accurately. Therefore, to obtain reliable predictions of wall heat flux during Stardust reentry, it is necessary to use the laminar flow model that accounts for surface viscosity and boundary layer phenomena.

4.4 Surface forebody pressure distributions

Figure 7 presents the surface pressure distribution over the forebody of the Stardust capsule for different wall conditions. As expected, the pressure reaches its maximum at the stagnation point and decreases along the body. The results show that pressure is largely insensitive to wall catalyticity and emissivity, confirming that surface pressure is primarily governed by the outer flow.

The pressure profiles are consistent with the reference data from [4] and [5]. However, a slight mismatch in surface length suggests that the geometry used in the present meshing may differ marginally from that employed in the reference studies, likely due to variations in the modeled capsule contour.

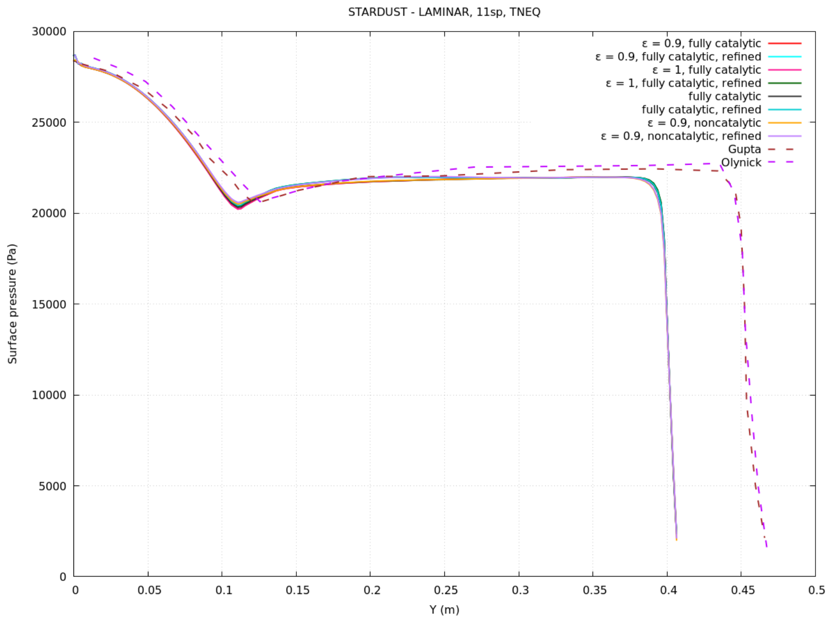

Figure 7: Surface forebody pressure profiles for various wall conditions

4.5 Temperature distributions along the stagnation streamline

The temperature distributions along the stagnation line are shown in Figure 8, distinguishing between translational and vibrational modes.

The shock position and post-shock values shown in Figure 8a exhibit good agreement with the results reported in [5], indicating consistent shock resolution. However, the peak values predicted by NSMB are noticeably higher than those in the reference data. This discrepancy may stem from differences in numerical modeling assumptions, grid resolution near the stagnation region, or the fact that Olynick et al. used NASA's GIANTS (Generalized Implicit Algorithm for the Navier-Stokes Transport Systems) code.

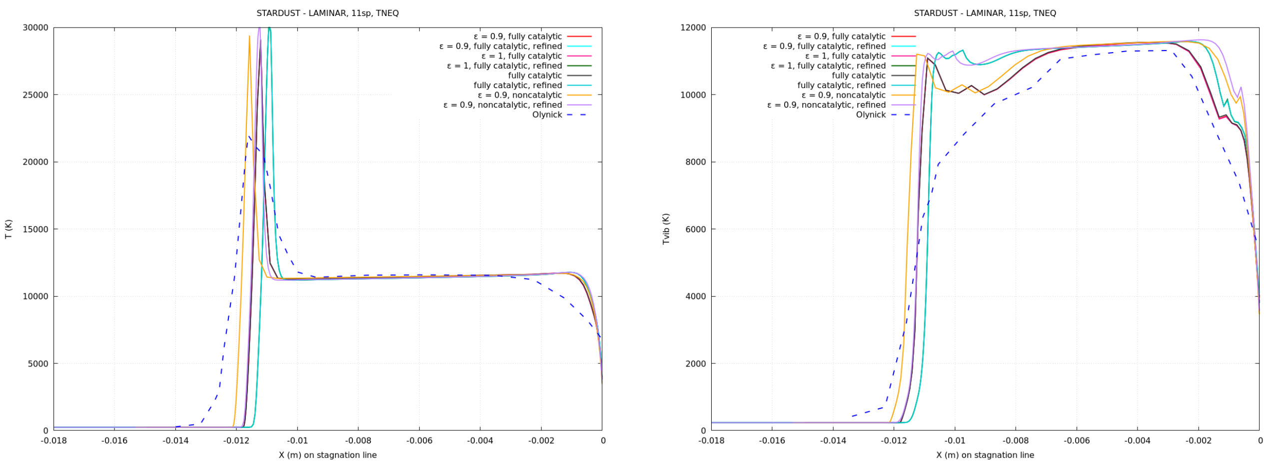

(a) Translational (b) Vibrational

Figure 8: Temperature profiles along the stagnation line

The vibrational temperature profiles of Figure 8b are consistent with Olynick et al.'s findings across all models. The NSMB simulations show again slightly higher vibrational peak temperature values, but the overall profile shape and behavior remain similar, with only minor variations.

4.6 Heat flux distribution along the capsule skin

The distribution of the total wall heat flux is examined under varying wall conditions in terms of catalyticity and emissivity as well as grid refinement in Figure 9.

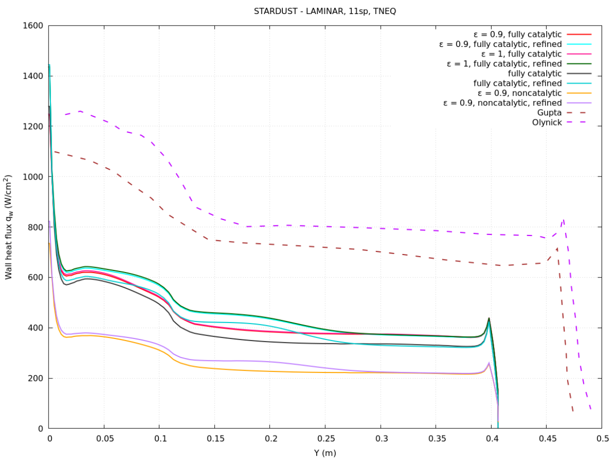

(a) Along Y direction

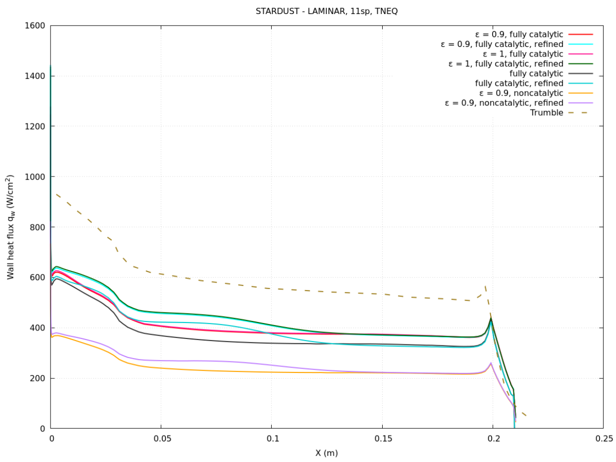

(b) Along X direction

Figure 9: Total wall heat flux for various wall conditions

The geometrical mismatch previously discussed is once again apparent in Figure 9a. Among the NSMB models, the fully catalytic configurations with radiation ($\epsilon = 0.9$ and blackbody radiation with $\epsilon = 1$) yield the best agreement with the results of Gupta [4] and Olynick [5] near the stagnation point. However, further downstream along the capsule's surface, significant deviations in the heat flux values arise between these models. The origin of these discrepancies remains unclear and may be linked to differences in radiation modeling or surface chemistry assumptions.

As shown in Figure 9b, the total wall heat flux along the capsule's symmetry axis (X-direction) reveals large discrepancies between the NSMB predictions and those reported by Trumble et al. [6]. Interestingly, the models tend to converge beyond $X = 0.2\,\text{m}$, following similar trends. This behavior is not fully understood and likely stems from differences between the solvers used, as Trumble employed NASA's DPLR (Data-Parallel Line Relaxation) code.

4.7 Mass fraction distributions along the stagnation streamline

The mass fraction profiles of key species (both neutral and ionized) were evaluated along the stagnation streamline. These include atomic and molecular nitrogen (N, N^+, N_2, $N_2{}^+$), nitric oxide (NO, NO^+), atomic and molecular oxygen (O, O^+, O_2, $O_2{}^+$), and electrons (e$^-$).

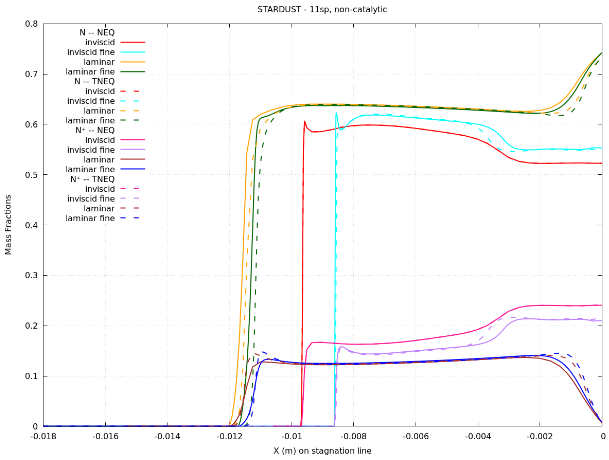

(a) N and N^+

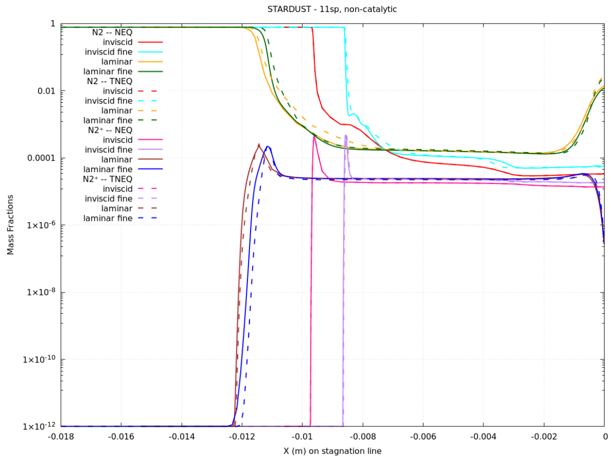

(b) N_2 and $N_2{}^+$

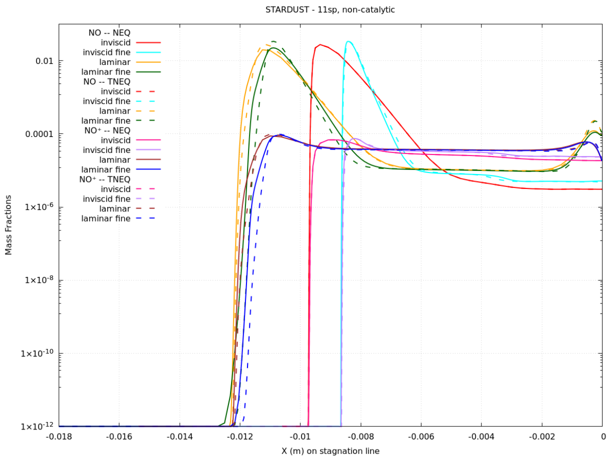

(c) NO and NO^+

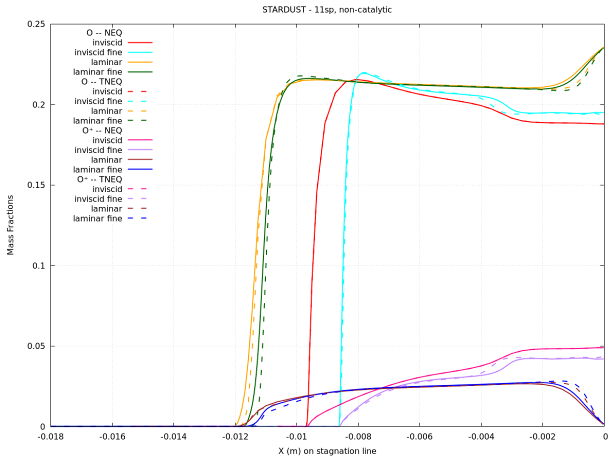

(d) O and O^+

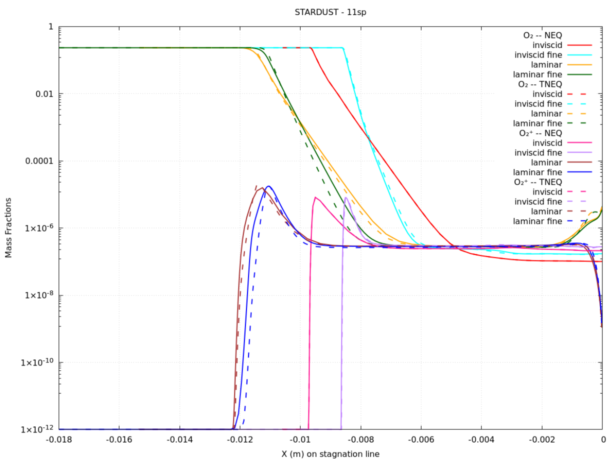

(e) O_2 and $O_2{}^+$

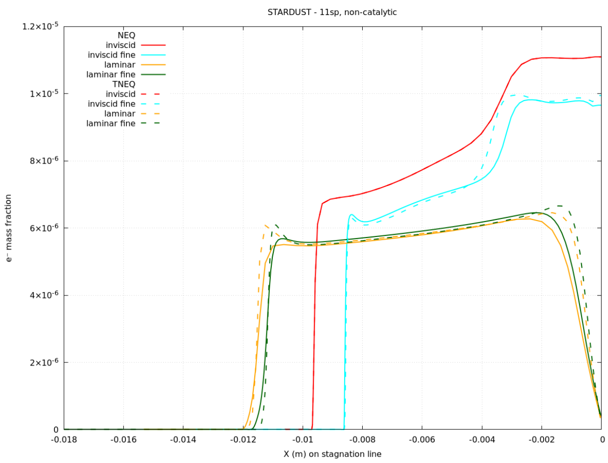

(f) e$^-$

Figure 10: Mass fraction profiles along the stagnation streamline

Although no reference data is available in the literature for validation of Figures 10a to 10f, the influence of grid refinement (baseline versus refined mesh) and the choice of flow modeling can be discussed.

Results show near-identical behavior within the same flow model when comparing the chemical non-equilibrium (solid lines) and thermo-chemical non-equilibrium (dashed lines of the same color) simulations. This suggests that the inclusion of thermal non-equilibrium has a limited impact on the mass fractions. In contrast, noticeable differences arise between laminar and inviscid models. These discrepancies are expected, as the viscous effects in laminar flows contribute to boundary layer formation and thermal diffusion, both of which are absent in inviscid formulations but play a crucial role in shaping species mass fraction distributions.

Moreover, comparisons between the baseline and refined grid results show only slight differences in values, while overall trends and profiles remain consistent. This suggests that the baseline grid has sufficient resolution to capture the main flow features, as shown by the good agreement in the shock layer and near the surface. Therefore, it can be considered accurate enough to be used for the following analyses.

4.8 3D geometry

The simulation began with a 2D axisymmetric model, but due to the appearance of the carbuncle phenomenon for certain configurations, a 3D quarter-symmetry model was adopted for the rest of the study. Multiple iterations of the 3D mesh were tested, including baseline, boundary-layer-resolved, non-boundary-layer and globally refined versions.

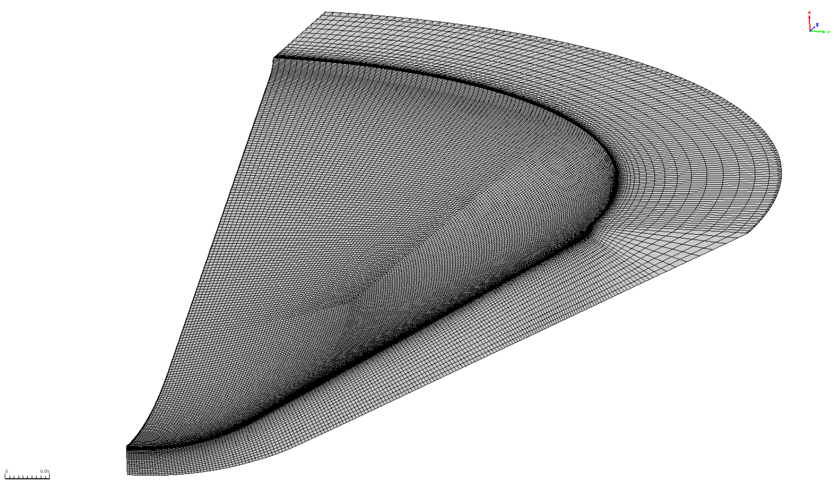

Figure 11: 3D mesh

This section assesses the sensitivity of heat flux predictions to the choice of viscosity (Blottner–Eucken vs. Gupta–Yos)and wall catalyticity models (non-catalytic, fully catalytic and finite-rate using Stewart&Al and VKI fits [1]), with comparisons to [8, 6, 4, 5]. It should be noted that the reference curves from Gupta and Olynick are over two decades old; their relevance for comparison should therefore be considered with caution, as CFD methodologies have significantly advanced since then. In contrast, Alkandry's data is more recent.

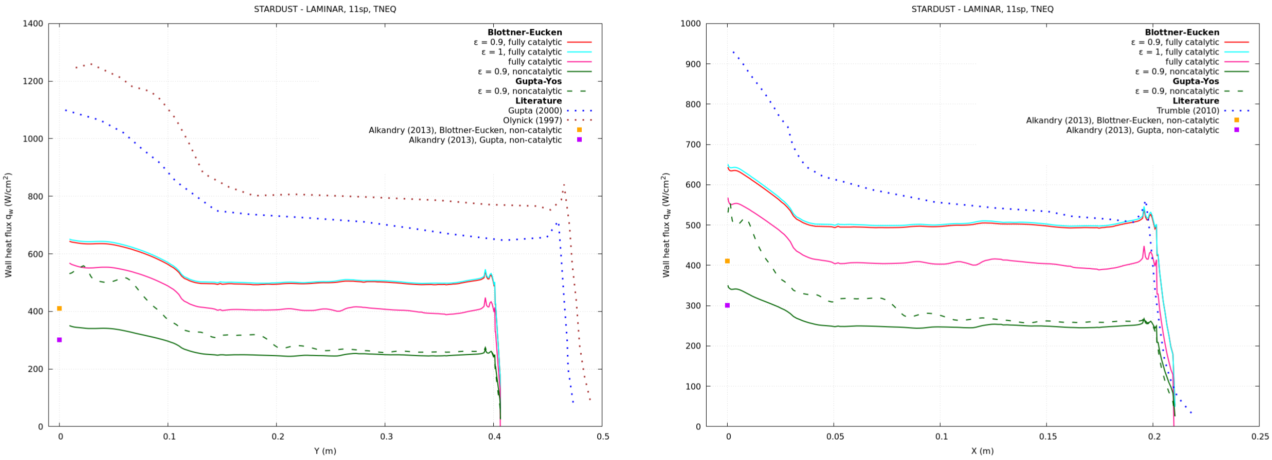

(a) Along the y-direction (b) Along the x-direction

Figure 12: Wall heat flux profiles for different viscosity models

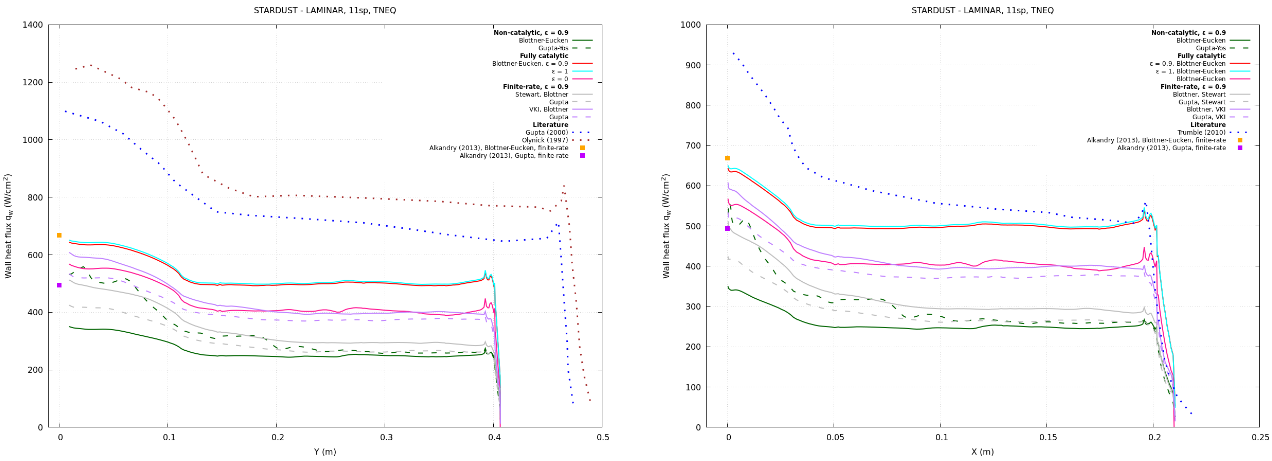

(a) Along the y-direction (b) Along the x-direction

Figure 13: Wall heat flux profiles for different surface chemistry models

The Blottner-Eucken and Gupta-Yos viscosity models lead to significant differences in predicted heat flux as shown in Figure 12. For a non-catalytic, radiative wall, the Gupta–Yos model increases heat flux by approximately 30–40% compared to Blottner–Eucken, but results in lower values for a partially catalytic, radiative wall.

Figure 13 highlights that catalyticity strongly influences the heat flux magnitude. Fully catalytic walls yield the highest heat flux levels, as recombination reactions at the surface release additional energy into the boundary layer. In contrast, non-catalytic conditions significantly reduce q_w, particularly when combined with Blottner-Eucken. Partial catalytic conditions predict intermediate values, as expected, close to the fully catalytic case for Blottner-Eucken but more distinct for Gupta-Yos.

The numerical results are compared with experimental and computational references (Alkandry, Olynick, and Gupta). Blottner-Eucken with fully catalytic walls provides the closest agreement with Alkandry's data near the stagnation point, although an overall underprediction remains when compared with Olynick's higher heat flux levels.

Implementation of the Gupta–Yos model with a fully catalytic wall encountered issues, leading to non-physical heat flux values and unusable results. Including this case would have been valuable for a complete comparative analysis.

4.9 TPS ablation

An attempt was made to simulate TPS ablation by coupling NSMB with the MUTATION++ library [9]. However, the results were inconclusive, and thus have been excluded from further analysis.

5 Conclusions

The numerical investigation conducted in this study confirms the critical role of thermochemical non-equilibrium and radiation modeling in accurately predicting the aerothermal environment experienced by the Stardust reentry capsule. Simulations using the NSMB solver, combined with an 11-species air model, show good agreement with available reference data, particularly regarding surface heat flux and temperature distributions near the stagnation point.

The analysis reveals that laminar flow models incorporating surface viscosity are essential for capturing boundary layer effects and producing realistic heat transfer predictions. While thermal non-equilibrium had limited impact on species mass fractions, it remains the most accurate model to consider at this velocity and altitude.

Grid refinement had only a minor influence on the key results, suggesting that the baseline mesh is adequate for the present case. However, discrepancies observed downstream and in total heat flux indicate ongoing challenges in modeling radiation and surface chemistry effects, highlighting the need for continued development of physical models and validation datasets.

Overall, this work reinforces the necessity of detailed physical modeling when simulating high-enthalpy reentry flows and demonstrates the value of benchmark cases like Stardust in advancing the accuracy of CFD tools used in atmospheric entry research.

References

[1] Hoarau, Y., Pena, D., Vos, J. B., Charbonnier, D., Gehri, A., Braza, M., Deloze, T., and Laurendeau, E., *Recent developments of the Navier–Stokes Multi Block (NSMB) CFD solver*, AIAA SciTech, San Diego, CA, Jan. 4–8, 2016. DOI: 10.2514/6.2016-2056.

[2] Kim, J. G., and Jo, S. M., *Modification of chemical-kinetic parameters for 11-air species in re-entry flows*, International Journal of Heat and Mass Transfer, Vol. 173, 2021, Article 121221. DOI: 10.1016/j.ijheatmasstransfer.2021.121221.

[3] Desai, P. N., Lyons, D. T., Tooley, J., and Kangas, J., *Entry, Descent, and Landing Operations Analysis for the Stardust Re-Entry Capsule*, AIAA Paper 2006-6410, AIAA Atmospheric Flight Mechanics Conference, Keystone, CO, Aug. 2006.

[4] Gupta, R. N., *Aerothermodynamic Analysis of Stardust Sample Return Capsule with Coupled Radiation and Ablation*, Journal of Spacecraft and Rockets, Vol. 37, No. 4, 2000, pp. 507–514.

[5] Olynick, D., Ghent, Y.-K., and Tauber, M. E., *Forebody TPS Sizing with Radiation and Ablation for the Stardust Sample Return Capsule*, AIAA Paper 1997-2474, 32nd Thermophysics Conference, Atlanta, GA, June 1997. DOI: 10.2514/6.1997-2474.

[6] Trumble, K. A., Cozmuta, I., Sepka, S., Jenniskens, P., and Winter, M., *Postflight Aerothermal Analysis of Stardust Sample Return Capsule*, Journal of Spacecraft and Rockets, Vol. 47, No. 5, Sept.–Oct. 2010, pp. 713–722. DOI: 10.2514/1.41514.

[7] Mitcheltree, R. A., Wilmoth, R. G., Cheatwood, F. M., Brauckmann, G. J., and Greene, F. A., *Aerodynamics of Stardust Sample Return Capsule*, NASA Langley Research Center, Hampton, VA, 1999. Presented at the AIAA Atmospheric Flight Mechanics Conference. AIAA Paper 1999-0306.

[8] Alkandry, H., Boyd, I. D., and Martin, A., *Comparison of Models for Mixture Transport Properties for Numerical Simulations of Ablative Heat-Shields*, Proceedings of the 51st AIAA Aerospace Sciences Meeting Including the New Horizons Forum and Aerospace Exposition, Paper 2013-0303, 2013, pp. 1–18. DOI: 10.2514/6.2013-303.

[9] James B. Scoggins, Vincent Leroy, Georgios Bellas-Chatzigeorgis, Bruno Dias, and Thierry E. Magin, "Mutation++: MUlticomponent Thermodynamic And Transport properties for IONized gases in C++," *SoftwareX*, vol. 12, 2020, doi: 10.1016/j.softx.2020.100575.